

Suction vortices and spiral breakdown in numerical simulations of tornado-like vortices

Brian Fiedler*

Professor of Meteorology, School of Meteorology, University of Oklahoma, 120 David L. Boren Blvd., Norman, OK 73072-7307, USA

*Correspondence to:
Brian Fiedler, Professor of
Meteorology, School of
Meteorology, University of
Oklahoma, 120 David L. Boren
Blvd., Norman, OK 73072-7307,
USA.
E-mail: bfiedler@ou.edu

Abstract

Three-dimensional simulations of tornado-like vortices are presented. The simulations are from a numerical model of the incompressible Navier-Stokes equations, with a Reynolds number, based on scales of the entire recirculating updraft, of up to 4.0×10^4 . In a companion axisymmetric model, the theory for the corner flow swirl ratio provides an excellent prediction of the results. For the three-dimensional nonaxisymmetric model, the corner flow swirl ratio is not easily applied *a priori*, but nonetheless provides a framework for identifying a consistent departure of the three-dimensional simulations from the axisymmetric simulations. Copyright © 2009 Royal Meteorological Society

Keywords: tornado; numerical simulation

Note: in this version, high-resolution graphics were restored with Nitro pdf

Received: 8 December 2008
Revised: 29 January 2009
Accepted: 29 January 2009

1. Introduction

Three-dimensional simulations of laminar vortices under a perpetual buoyancy updraft were presented in Fiedler (1998). The vortices were offered as idealized tornadoes, from which a relationship between the environment and the maximum wind speed could be learned. These simulations are being updated with modern computing power, for the purpose of further refining the knowledge of the factors that control maximum wind speed, and towards that purpose the recent developments in the concept of corner flow swirl ratio have been fruitfully applied. Simulations are quadruple in both resolution and Reynolds number, as compared with those used in Fiedler (1998). The current simulations commonly contain intense suction vortices capped by a spiral vortex breakdown. Spiral breakdown has been studied in an engineering context (e. g. Serre and Bontoux, 2002; Lim and Cui, 2003). Those studies have not been focused on its role in maintaining, or limiting, the strong winds at the base of a tornado. That role is the focus in the current study. These simulations do not employ parameterized turbulence, as in Xia *et al.* (2003).

The conclusion in Fiedler (1998) stated: “*These results are exactly in line with the deduction of Fujita (1971), who estimated that a suction vortex would have a wind speed twice that of the parent vortex*”. As perhaps could be anticipated, these simulations at higher resolution and Reynolds number reveal a greater frequency of events that exceed the doubling of wind speed deduced by Fujita (1971). Enhancement beyond doubling is also reported in Lewellen and Lewellen (2007a,b).

Figure 1 shows two still images captured from high-definition video taken by storm chasers Reed

Timmer and Joel Taylor in 2007. The combination of a close vantage point and the absence of obscuring dust provided an exceptional record of suction vortices indicated by condensation, allowing the low pressure of the suction vortices to be clearly inferred. However, a view of the point of contact with the surface is apparently obscured by a slight dip in the terrain.

Though the suction vortices in Figure 1(b) are multiple, this tornado would usually not be regarded as a multiple-vortex tornado, such as the one providing illustration in Bluestein (2007). As seen from the farther vantage point of Figure 1(a), the tornado is a classic single vortex. Note there is a hint of a suction vortex at the base of the tornado as seen in Figure 1(a). But only an uncommonly close observer could witness the multiplicity of suction vortices, as seen at close approach in Figure 1(b). The multiple-vortex phenomenon studied in a laboratory chamber by Church *et al.* (1979) is often a larger scale phenomenon, with multiple vortices dominating the depth of the chamber. Most of the simulations here, however, show single or multiple suction vortices at the base of a vortex that appears to be single aloft, similar to the tornado in Figure 1.

2. The model

The numerical simulations are configured as in Fiedler (1998). The numerical model is dimensionless. The domain is a box $4 \times 4 \times 1$ with a permanent central buoyancy field that, acting alone, would accelerate a parcel to one unit of velocity along the central axis of the model. Alternatively, the central buoyancy field could support a hydrostatic pressure deficit of one-half unit at the surface. That hydrostatic pressure



Figure 1. Ellis County, OK tornado of May 4, 2007. Photos courtesy of Reed Timmer and Joel Taylor of TornadoVideos.net. Image (a) is from approximately 1 km away, a few minutes before the viewing at approximately 100 m in the (b) image. Suction vortices are evident at the base of the condensation funnel.

deficit could balance a wind speed of one unit in a surrounding stagnant-core potential vortex.

The grid typically employed $181 \times 181 \times 91$ grid points. The grid is greatly stretched in both the vertical and horizontal. At the surface, the horizontal grid widths Δx and Δy are less than 0.0054 in the region $-0.2 < x < 0.2$ and $-0.2 < y < 0.2$, where the tornado forms. The grid is stretched in the vertical to enhance the resolution in the viscous boundary layer, leaving $z = 0.0022$ at the lowest level. The model has fifth-order, upwind-biased advection. An iterative solver maintains a close approximation to incompressibility. As was also done in Fiedler (1998), a companion axisymmetric model in a cylinder, of radius 2 and height 1, is used for comparison with the three-dimensional experiments in a box.

The dimensionless viscosity μ is a constant below $z = 0.5$, either 4.0×10^{-4} , 1.0×10^{-4} or 2.5×10^{-5} . Above $z = 0.5$, μ increases linearly to 0.001 at the top boundary at $z = 1$, to create a damping region in the upper domain. With the height of the domain one unit and the buoyancy-driven velocity scale one unit, μ in the lower half of the domain (the region of interest) could be referred to as the inverse Reynolds number

of the simulation. The code allows for interpolation onto a double resolution grid, and restarting of the simulation. For $\mu = 2.5 \times 10^{-5}$, a $361 \times 361 \times 181$ grid sometimes yields suction vortices that are 20% more intense. However, for the two larger μ , there was negligible increase in wind speed at this higher resolution. Some of the statistics reported later for $\mu = 2.5 \times 10^{-5}$ are from these highest-resolution simulations, meaning from a restarted simulation, for a shorter time period of interest. Nevertheless some of the highest wind speed structures reported for $\mu = 2.5 \times 10^{-5}$ are reproducible with either resolution, meaning $181 \times 181 \times 91$ is adequate.

The lower boundary is no-slip, the other boundaries are free-slip. A dimensionless Coriolis force, designated with the usual parameter f , provides the source of the vertical relative vorticity. In the simulations shown here, f varies from 0 to 0.20. Given the width of the simulated vortices is at most 0.1, the Rossby number of these simulations is at least 100. Thus the rotation of the coordinate system is simply a convenient way to provide a source of vertical vorticity that can be stretched and amplified in a central vortex. Except for that, the Coriolis force has negligible effect on the dynamics of the central vortex.

3. Intensity summary

Figure 2 summarizes the minimum pressure ϕ_{\min} (pressure divided by density, normalized by velocity scale squared) in the central vortices. The central buoyancy field by itself could sustain $\phi_{\text{hydro}} = -1/2$ at the surface, by hydrostatic means. The ratio of these quantities is plotted as,

$$I_p = \sqrt{\frac{\phi_{\min}}{\phi_{\text{hydro}}}} \quad (1)$$

where I_p , a measure of the intensification of pressure, is being used as in Lewellen and Lewellen (2007a). The statistics are gathered for $t > 100$, well after the initial transient response documented in Fiedler (1998). Statistics from the $361 \times 361 \times 181$ simulations may be for a time interval as small as $\Delta t = 1$, in a simulation restarted by interpolation onto this high resolution grid. Nevertheless, $\Delta t = 1$ allows for several complete orbits of the suction vortex within the parent vortex.

Lewellen and Lewellen (2007a) offer a figure similar to Figure 2, together with a prediction from an analytic model, based on the corner flow swirl ratio S_c . An analysis of Figure 2 is given in the following sections, after a review of S_c .

4. Corner flow swirl ratio

Lewellen *et al.* (2000) introduce a dimensionless parameter, based on properties of the surface boundary

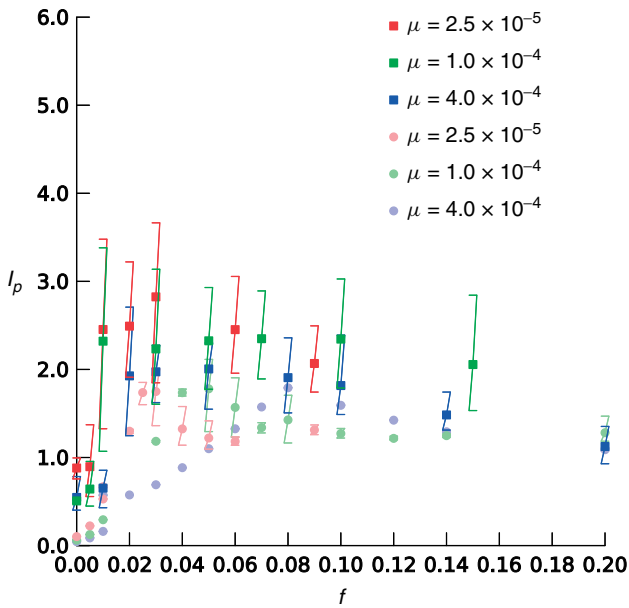


Figure 2. Summary of the maximum pressure deficit I_p in simulations with various dimensionless viscosity μ and dimensionless Coriolis parameter f . Square symbols were three-dimensional simulations within a box. Circular symbols were axisymmetric simulations within a cylinder. 95% of the recorded values are above the low end of the error bar and 5% of the recorded values are above the high end. The central symbol is the mean of the recorded values.

layer flowing into a vortex. The parameter essentially predicts properties of the ensuing central vortex. The parameter is the *corner flow swirl ratio*:

$$S_c = \frac{r_c \Gamma_\infty^2}{\Upsilon} \quad (2)$$

where Γ is the angular momentum, per unit mass, about the center line and Γ_∞ is the ambient value, undisturbed by friction. Υ is the depleted angular momentum flux

$$\Upsilon = - \int_0^{z_1} 2\pi r u (\Gamma_\infty - \Gamma) dz \quad (3)$$

where u is the radial velocity component and the integral is over the depth of the inflowing boundary layer.

The numerator in Equation (2) can be interpreted as proportional to the *vertical* depleted angular momentum flux in a supercritical flow of maximum intensity. Firstly, r_c is the radius to which fluid with angular momentum of Γ_∞ could penetrate and achieve a swirl velocity V_c :

$$r_c = \frac{\Gamma_\infty}{V_c} \quad (4)$$

where V_c is a dynamical speed limit on the upper portion of the vortex. Secondly, in a loss-free corner flow, the resulting upward velocity component w_c will be proportional to V_c , with a proportionality constant that is in fact the subject of this article. The depleted angular momentum flux up the core will be

proportional to $w_c r_c^2 \Gamma_\infty$, or $V_c r_c^2 \Gamma_\infty$, which is the numerator of Equation (2). S_c is thus a measure of the ability of the inflowing boundary layer to adequately supply the core with upward moving fluid depleted of angular momentum, consistent with the constraint on the downstream core size r_c , or equivalently the speed limit V_c .

If S_c is greater than a critical value S_c^* , which Lewellen and Lewellen (2007a) find to be between 0.70 and 1.78, then a high-swirl vortex results, with a central downdraft. If S_c is less than the critical value, then a low-swirl vortex results, with a core wider than r_c and swirl velocity less than allowed by the speed limit V_c . When S_c is at or near the critical value S_c^* , a vortex with strong axial flow can exist, with the strong axial flow terminating in a vortex breakdown close to the surface. This configuration produces the maximum intensity I_p of the vortex (for a given V_c).

The coupling of the inflowing boundary layer to the core of a tornado vortex was also investigated by Fiedler and Rotunno (1986). The boundary layer was that induced by a potential vortex (one with constant Γ_∞ above it) as presented by Burggraf *et al.* (1971), applied at the high Reynolds number limit. From that limit, we can calculate

$$\Upsilon = B \delta \Gamma_\infty^2 \quad (5)$$

where $B = 2.63$. δ is the depth of the boundary layer as $r \rightarrow 0$:

$$\delta = r_b \sqrt{\frac{\nu}{\Gamma_\infty}} \quad (6)$$

where ν is the kinematic viscosity and r_b is the radius at which the boundary layer begins to form. So from Equations (2) and (5):

$$S_c = \frac{r_c}{B \delta} \quad (7)$$

Fiedler and Rotunno (1986) found that the supercritical end-wall vortex that erupts from the boundary layer has a swirl velocity $v_1 = 0.51 \Gamma_\infty \delta^{-1}$. Downstream of the breakdown point $v_2 = 0.25 \Gamma_\infty \delta^{-1}$. (The number 0.25 depending somewhat on assumptions about the distribution of the dissipation). If the flow past the vortex breakdown matches to downstream conditions, or $v_2 = V_c$, then Equation (4) shows $r_c = 4.0 \delta$. Using these conditions, Equation (7) yields $S_c^* = 1.523$.

More generally, for conditions other than the optimal, combining Equations (6) and (4) with Equation (7) gives:

$$S_c = \Gamma_\infty^{\frac{3}{2}} \nu^{-\frac{1}{2}} \frac{1}{2} B^{-1} r_b^{-1} V_c^{-1} \quad (8)$$

In the dimensionless model, angular momentum is provided by the rotation of the coordinate system, and will have a dimensionless value of $\frac{1}{2} f R^2$, where R is the dimensionless radius of the source of fluid

where the relative swirl velocity is near 0. Applying Equation (8) to the dimensionless model, v should be replaced by the inverse Reynolds number μ and Γ_∞ by $\frac{1}{2}f R^2$. Likewise, R , r_b and V_c should be replaced by values of order 1. If the above conditions are met (and they evidently are in the axisymmetric model):

$$S_c = c f^{\frac{3}{2}} \mu^{\frac{-1}{2}} \quad (9)$$

where c will be of order 1. Nevertheless, c should not be expected to be a universal constant, as both R and r_b should be expected to depend on the geometry of the domain and the forcing, as, for example, implied by Nolan (2005).

For a given μ we can solve for f that produces the peak intensity at $S_c = S_c^*$:

$$f = \alpha \mu^{\frac{1}{3}} \quad (10)$$

where

$$\alpha = (c^{-1} S_c^*)^{\frac{2}{3}} \quad (11)$$

Given the statements about c and S_c , we expect that a value of α close to 1 will be consistent with the experiments. In fact, a value of $\alpha = 1$ gives an excellent prediction in the axisymmetric simulations. For the three increasing values of μ used in the simulations, we see in Figure 2 a peak in I_p at 0.03, 0.05 and 0.08. Using $\alpha = 1$ in Equation (10) predicts the peaks to be at 0.029, 0.046 and 0.073.

Note that Equation (9) can be written as

$$S_c = c \left(\frac{f}{\mu}\right)^{\frac{3}{2}} \mu \quad (12)$$

where the quantity in parentheses is essentially the vortex Reynolds number that was identified by Nolan (2005) to have the significant control of vortex structures. That claim would be consistent with the primacy of S_c , if μ is held invariant.

5. The three-dimensional simulations

Figures 3, 4 and 5 depict the central vortex in the model using renderings of isosurfaces. In all simulations, the primary vortex flow is anticlockwise. Spiral structures of low pressure wind clockwise with height. The images are not selected to show a clean progression of vortex structure from the classic low-swirl to high-swirl structure, as could be shown for steady-state axisymmetric vortices. Rather, for a broad range of f , the model episodically produces suction vortices. Even for a fixed f , an episode of growth and decay of a suction vortex may exhibit low-swirl structure (a long vortex of supercritical flow with an elevated vortex breakdown) to high-swirl structure (no supercritical flow and a central downdraft). Structures with supercritical flow, and high intensity, are emphasized in the images.

Unlike the axisymmetric model, the three-dimensional model can produce a weak, concentrated vortex with $f = 0$. Such a vortex is shown in Figure 3(a), showing a low-swirl structure. Viscous stresses on the lower boundary of the box, combined with the fact that the box has corners, provides for the generation of vertical vorticity. Round-off error is able to perturb the symmetry imposed by the four corners, and one vortex can come to dominate the flow.

Many of the renderings in Figures 3 through 5 show a low-pressure structure close to the lower boundary,

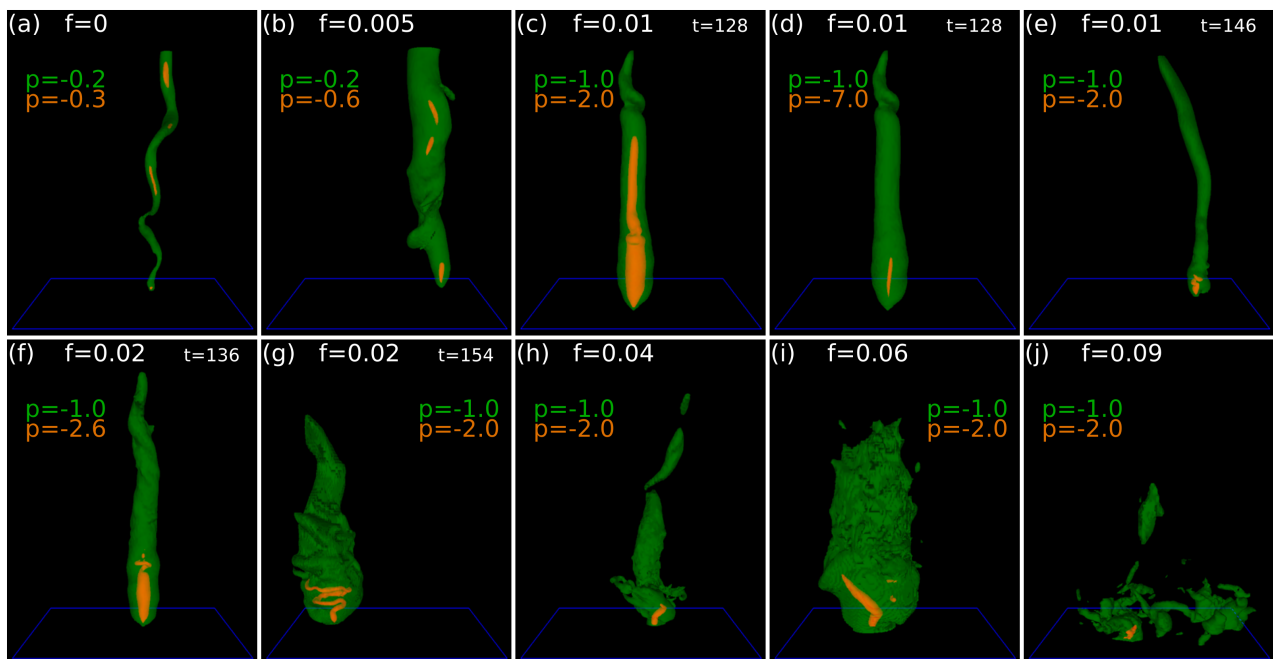


Figure 3. Low viscosity, $\mu = 2.5 \times 10^{-5}$ simulations. Isosurfaces of pressure in simulated vortices for various f . The time t is indicated if more than one figure is shown for a particular f . For perspective and size reference, the blue square marks a 0.4×0.4 area on the lower boundary. The area is centered, except for the $f = 0$ case, where the rear edge is centered.

Spiral breakdown in tornadoes

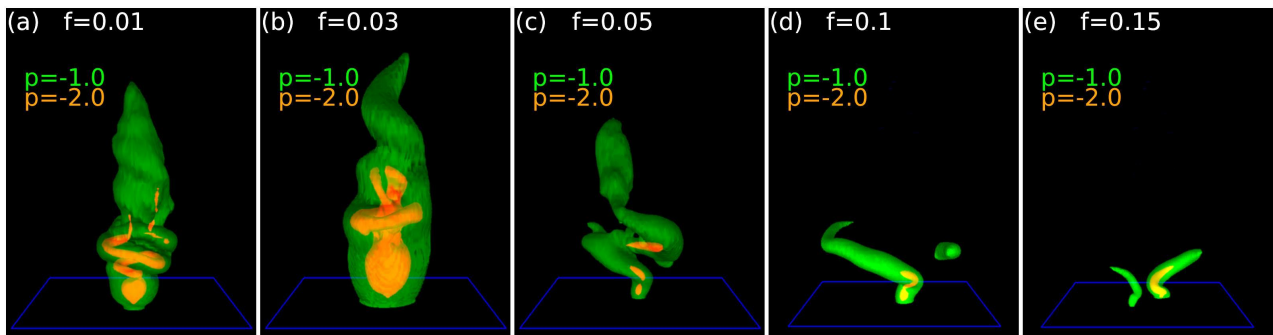


Figure 4. Medium viscosity, $\mu = 1.0 \times 10^{-4}$ simulations. Isosurfaces of pressure in simulated vortices for various f .

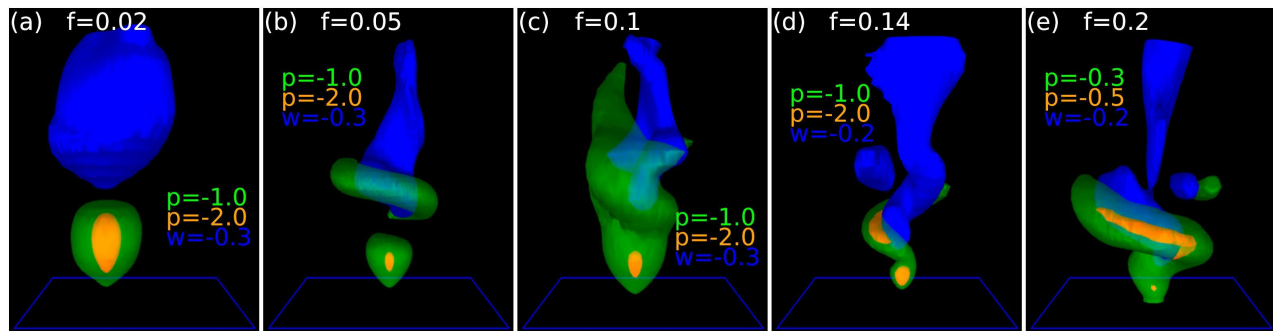


Figure 5. High viscosity, $\mu = 4 \times 10^{-4}$ simulation. Isosurfaces of pressure in simulated vortices for various f . An isosurface of a negative value of vertical velocity w is rendered to show the central downdraft. (A central downdraft also occurs in many of the simulations depicted in Figure 3 and Figure 4, but was not shown for reasons of clarity).

which may consist of either an orange bulb or shaft, capped by a spiral. Figures 3(e), 4(a) and 5(b) show tidy examples of this bulb-spiral description. When investigated for lower pressure isosurfaces, this bulb invariably contains the lowest pressure in the domain. It will also contain a vertical jet, with the largest velocity in the domain. These axial jets, in the center of these so-called *suction vortices*, have been noted in previous three-dimensional models of tornadoes, but a spiral structure capping the jet is rarely presented. For example, in Lewellen and Lewellen (2007b), azimuthal averages are emphasized, which preserve the axial-jet, but remove any spiral structure.

Lewellen *et al.* (2000) show a simulation of a high-swirl vortex containing seven secondary vortices. Figure 1(b) shows indications of three vortices being present. Except for Figure 4(f), the investigation of these simulations did not readily provide clean examples of such symmetric multiple vortices. Whether this lack is because the Reynolds number is too low, or the stretched grid is inadequate for wider, high-swirl vortices, cannot be stated.

6. Conclusion

The conclusions about the axisymmetric simulations are as follows. S_c is shown here to be a successful single predictive parameter of tornado structure. S_c is entirely calculable from the model configuration parameters, primarily μ and f . For the factor of 16 range in μ , there was no significant variation in

I_p at $S_c = S_c^*$, consistent with the theoretical independence of I_p from μ . Furthermore, this value of $I_p \approx 2$ is satisfactorily given by theoretical analysis of properties of axisymmetric supercritical flow, as studied by Fiedler and Rotunno (1986) and Lewellen and Lewellen (2007a). In summary, for the axisymmetric cases, for the Reynolds numbers investigated here, there is little that is unexplained.

The three-dimensional simulations have more transient events. The average I_p is greater than in the corresponding axisymmetric simulation. The peak intensity occurs at a lower value of f , as compared with the axisymmetric simulations. Unlike the axisymmetric simulations, S_c is not calculable from model parameters: Equation (9) assumed axisymmetric properties. In principle, S_c could be diagnosed for the individual three-dimensional events, but that was not done here. Nevertheless, the theory for S_c provides a possible explanation for the shift to lower f : the boundary layer depth (the role played by δ) is thinner for the transient, orbiting suction vortices than for the axisymmetric vortices.

There is also a shift toward higher intensity with increased Reynolds number. The reasons are not known with certainty, but Fiedler (1997) cautions about monitoring wind speed maxima. The statistical theory for turbulence – even in a gentle breeze – allows for rare supersonic events, especially on small space and time scales. Numerical simulations progressing to increased Reynolds number and resolution may produce reports of higher wind speed events, as is the case here, but these events may be on smaller

spatial scales. Monitoring averages from a fixed sampling volume might reveal less of an increase in peak wind speed as Reynolds number increases, but that was not done here.

Putting aside this sampling issue, the results indicate an intensification rule for supercritical vortex flow. Coupling to downstream conditions via a spiral vortex breakdown appears to be quantitatively similar to coupling via a vortex breakdown forced to remain axisymmetric. The three-dimensional simulations have an $I_p \approx 2.5$ (and occasionally much greater than that in transient events) over a broad range of f , while the axisymmetric simulations have $I_p \approx 2.0$, but over a narrow range of f . Such magnitudes of I_p are similar to simulations of Lewellen and Lewellen (2007a), which have parameterized subgrid mixing.

For the present model to simulate the Reynolds number of a thunderstorm, another factor of 10^6 in Reynolds number would be needed. Such simulations may not reveal anything new. These current simulations at low Reynolds number, and those of Lewellen and Lewellen (2007a) at high Reynolds number (with parameterized turbulence), show behavior that is consistent with observations of tornado structure and wind speed near the ground (Bluestein, 2007). Dynamical explanations for tornado structure and wind speed near the ground are not wanting.

Knowledge of S_c , together with knowledge of intensification processes associated with various regimes of S_c , does, in principle, allow for prediction of near-surface tornado intensity. However, acquiring S_c in a tornado event would be operationally more difficult than sensing the intensity itself. There is little, if any time lag, between the appearance of certain value of S_c and the associated intensity. Nevertheless, the science being built upon S_c could have substantial indirect impact on prediction of tornadoes by numerical weather prediction models. For example, such models may forecast well the storm structure and tornadogenesis sites, but otherwise misforecast tornado structure and intensity. This science will provide a focus for a remediation of these models, by directing focus on the model's sensitivity to near-surface turbulence parameterizations and especially the resulting sensitivity of S_c to those parameterizations and to model resolution.

Acknowledgements

This work was supported by National Science Foundation Grant ATM-0646914.

References

- Bluestein HB. 2007. Advances in applications of the physics of fluids to severe weather systems. *Reports on Progress in Physics* **70**: 1259–1323, DOI: 10.1088/0034-4885/70/8/R01.
- Burggraf OR, Stewartson K, Belcher R. 1971. Boundary layer induced by a potential vortex. *Physics of Fluids* **14**: 1821–1833, DOI:10.1063/1.1693691.
- Church CR, Snow JT, Baker GL, Agee EM. 1979. Characteristics of tornado-like vortices as a function of swirl ratio: a laboratory investigation. *Journal of the Atmospheric Sciences* **36**: 1755–1776, DOI: 10.1175/1520-0469(1979)036<1755:COTLVA>2.0.CO;2.
- Fiedler BH. 1997. Compressibility and wind speed limits in tornadoes. *Atmosphere-Ocean* **35**: 93–107.
- Fiedler BH. 1998. Wind-speed limits in numerically simulated tornadoes with suction vortices. *Quarterly Journal of the Royal Meteorological Society* **124**: 2377–2392, DOI: 10.1002/qj.49712455110.
- Fiedler BH, Rotunno R. 1986. A theory for the maximum windspeeds in tornado-like vortices. *Journal of the Atmospheric Sciences* **43**: 2328–2340, DOI: 10.1175/1520-0469(1986)043<2328:ATOTMW>2.0.CO;2.
- Fujita TT. 1971. Proposed mechanism of suction spots accompanied by tornadoes. *Preprints, Seventh Conference Severe Local Storms*, Boston, 208–213.
- Lewellen DC, Lewellen WS. 2007a. Near-surface intensification of tornado vortices. *Journal of the Atmospheric Sciences* **64**: 2176–2194, DOI: 10.1175/JAS3965.1.
- Lewellen DC, Lewellen WS. 2007b. Near-surface vortex intensification through corner flow collapse. *Journal of the Atmospheric Sciences* **64**: 2195–2209, DOI: 10.1175/JAS3966.1.
- Lewellen DC, Lewellen WS, Xia J. 2000. The influence of a local swirl ratio on tornado intensification near the surface. *Journal of the Atmospheric Sciences* **57**: 527–544, DOI: 10.1175/1520-0469(2000)057<0527:TIOALS>2.0.CO;2.
- Lim TT, Cui YD. 2003. On the generation of a spiral-type vortex breakdown in an enclosed cylindrical container. *Physics of Fluids* **17**: 044105, DOI: 10.1063/1.1872072.
- Nolan DS. 2005. A new scaling for tornado-like vortices. *Journal of the Atmospheric Sciences* **62**: 2639–2645, DOI: 10.1175/JAS3461.1.
- Serre E, Bontoux P. 2002. Vortex breakdown in a three-dimensional swirling flow. *Journal of Fluid Mechanics* **459**: 347–370, DOI: 10.1017/S0022112002007875.
- Xia J, Lewellen WS, Lewellen DC. 2003. Influence of Mach number on tornado corner flow dynamics. *Journal of the Atmospheric Sciences* **60**: 2820–2825, DOI: 10.1175/1520-0469(2003)060<2820:IOMNOT>2.0.CO;2.